Passive Properties and Membrane Currents of Canine Ventricular Myocytes

GEA-NY TSENG, RICHARD B. ROBINSON, and BRIAN F. HOFFMAN

From the Department of Pharmacology, College of Physicians and Surgeons, Columbia University, New York, New York 10032

ABSTRACT The membrane potential and membrane currents of single canine ventricular myocytes were studied using either single microelectrodes or suction pipettes. The myocytes displayed passive membrane properties and an action potential configuration similar to those described for multicellular dog ventricular tissue. As for other cardiac cells, in canine ventricular myocytes: (*a*) an inward rectifier current plays an important role in determining the resting membrane potential and repolarization rate; (*b*) a tetrodotoxin-sensitive Na current helps maintain the action potential plateau; and (*c*) the Ca current has fast kinetics and a large amplitude. Unexpected findings were the following: (*a*) in approximately half of the myocytes, there is a transient outward current composed of two components, one blocked by 4-aminopyridine and the other by Mn or caffeine; (*b*) there is clearly a time-dependent outward current (delayed rectifier current) that contributes to repolarization; and (*c*) the relationship of maximum upstroke velocity of phase 0 to membrane potential is more positive and steeper than that observed in cardiac tissues from Purkinje fibers.

INTRODUCTION

Single cardiac myocytes have been successfully isolated from many different species and tissues (ventricular myocytes from guinea pig, cow, rat, and cat: Powell and Twist, 1976; Isenberg and Klockner, 1982*a*; Josephson et al., 1984*a*, *b*; Houser et al., 1985; atrial myocytes from rabbit and guinea pig: Nakayama et al., 1984; Iijima et al., 1985; Purkinje cells from calf, sheep, and dog: Callewaert et al., 1984; Sheets et al., 1983; atrial myocytes from bullfrog: Hume and Giles, 1981). They have been useful in studying cardiac electrophysiology by allowing better voltage-clamp experiments and better control of external and internal ionic compositions and single channel recordings (Baumgarten et al., 1977; Hilgemann, 1986; Brown and Yatani, 1986). So far, there has not been any systematic study on dog ventricular myocytes, although many studies on cardiac ischemia, infarction, arrhythmias, and antiarrhythmic drugs have used dogs as

Address reprint requests to Dr. Gea-Ny Tseng, Dept. of Pharmacology, College of Physicians and Surgeons, Columbia University, 630 W. 168th St., New York, NY 10032.

J. GEN. PHYSIOL. © The Rockefeller University Press · 0022-1295/87/11/0671/31$2.00

Volume 90 November 1987 671–701

animal models (Reimer and Jennings, 1986). The many variations among tissues and species (Josephson et al., 1984*a*, *b*; Hume and Uehara, 1985) make a direct extrapolation from studies on other species or tissues to dog ventricular muscle difficult. Therefore, we undertook a thorough study on the passive properties and membrane currents of dog ventricular myocytes. Our results reveal some unexpected findings concerning the relationship between the maximum upstroke velocity of action potential phase zero and membrane potential, the existence of two transient outward current components, and the existence of delayed rectifier current. These have not been reported before and should be taken into account when studying dog ventricular muscle under different settings.

METHODS

Preparation of Single Cells

The cells were isolated by a method modified from that of Powell and Twist (1976), as previously reported (Hewett et al., 1983), but with two minor modifications: (*a*) after trituration, the cells were not washed, and (*b*) the cells were filtered only once through 160-μm nylon mesh after centrifugation. Cells from the fifth to seventh harvests were used for all studies. We allowed 3–5 min for the cells to adhere to a poly-*l*-lysine–coated glass coverslip placed on the bottom of a 0.7-ml Lucite tissue chamber, before starting continuous superfusion with Tyrode's solution with the following composition (millimolar): 137 NaCl, 12 $NaHCO_3$, 5.5 dextrose, 1.8 NaH_2PO_4, 0.5 $MgCl_2$, 4 KCl, and 2 $CaCl_2$, equilibrated with 95% O_2/5% CO_2 and maintained at pH 7.1, 35–37°C. The flow rate was 1.2 ml/min. For some experiments on Ca currents, we used an Na- and K-free external solution with the following composition (millimolar): 137 choline chloride, 5.5 dextrose, 0.5 $MgCl_2$, 2 or 5 $CaCl_2$ (as indicated), and 5 HEPES, adjusted to pH 7.4 with CsOH.

Electrophysiological Studies

We used two different methods to record and control membrane potential. To maintain a normal intracellular environment, for transmembrane potential recordings and voltage-clamp experiments on either the time-independent current or the transient outward current component that is activated by intracellular Ca (see Results), we used the switched-clamp technique with a single microelectrode and an amplifier (AxoClamp-2, Axon Instruments, Inc., Burlingame, CA). The switching rate was set between 1 and 10 kHz, depending on the microelectrode tip resistance. The form of the voltage signal before the sample-and-hold unit was monitored continuously to ensure that the voltage drop across the tip resistance subsided completely between current injection cycles. Microelectrodes were made from fiber-filled capillary tubing (1.2 mm o.d., Glass Company of America, Bargaintown, NJ) and filled with 3 M KCl solution; the electrode tip resistance was 30–50 MΩ and the tip potential was less than −10 mV. For experiments on the Ca current, the transient outward current component that is not dependent on intracellular Ca activity and the delayed rectifier current, we used the continuous-clamp method with a suction pipette, as described by Hamill et al. (1981). Pipettes were made of Pyrex glass (1 mm i.d., Mercer Glass, New York) with a two-stage puller (PE-2, Narishige Scientific Co., Tokyo, Japan). The pipettes were heat-polished before use and filled with one of two pipette solutions. The K-containing pipette solution had the following composition (millimolar): 125 K-aspartate, 20 KCl, 10 EGTA, 5 ATP (Mg salt), 1 $MgCl_2$, and 5 HEPES. The Cs-containing pipette solution had the following composition (millimolar): 125 Cs-aspartate, 20 tetraethylammonium chloride, 10 EGTA, 5 ATP (Mg salt), 1 $MgCl_2$, and 5

HEPES. The pH of the pipette solutions was adjusted to 7.3 with KOH for the K-containing solution and with CsOH for the Cs-containing solution. The Ca activity of the pipette solutions was <100 nM, as measured with a Ca electrode (Cal-1, World Precision Instruments, Inc., New Haven, CT), which had a selectivity coefficient of $10^{5.7}$ against K and, when calibrated with Calbuf Ca buffer solutions (World Precision Instruments, Inc.) (90 mM KCl, pH 7–9, pCa 1–8), had a slope of ~30 mV/decade change in Ca activity down to pCa 6 or 7. The tip size of the suction pipette was 3–5 μm and the tip resistance was 2–4 MΩ. The tip liquid junction potential between the pipette solution and the normal Tyrode's solution was determined by measuring the change in the tip potential between a pipette filled with normal Tyrode's solution and the pipette filled with the pipette solution. The junction potential was ~15 mV with either pipette solution (pipette solution negative). The voltages of continuous-clamp experiments using suction pipettes were corrected for this junction potential. For the continuous clamp with suction pipettes, the series resistance (R_s) was compensated for by scaling the current signals by a variable factor (r_2/r_1) and adding these scaled signals as positive feedback to the voltage command. The usual value of r_2/r_1 was 0.08–0.1. This, coupled with the 100-MΩ feedback resistor, gave a compensated R_s of 8–10 MΩ. With a pipette resistance of 2–4 MΩ, the total uncompensated R_s was 2–5 MΩ. For the transient outward current or Ca current, which had maximum amplitudes of ~1 nA, the voltage error was estimated to be 2–5 mV.

Data Acquisition and Analysis

During the experiments, data were continuously recorded on FM tape (model B, A. R. Vetter Co., Rebersburg, PA) at a speed of 7.5 ips (3-dB bandwidth: 0–2.2 kHz) for later analysis. Data were also continuously recorded on a chart recorder (Brush 2400, Gould Inc., Cleveland, OH) and displayed on an oscilloscope (565 or 5113, Tektronix, Inc., Beaverton, OR); at times, data were photographed from the oscilloscope with Polaroid film.

The taped data were replayed, and membrane currents were sampled by a 12-bit analog-to-digital converter (LabMaster, TecMar Scientific Solutions, Burlingame, CA). Depending on the current kinetics, the sampling time was between 0.1 and 10 ms. The data acquisition and initial analysis were controlled by pClamp programs (Axon Instruments, Inc.) and an IBM AT. Exponential curve-fitting was accomplished using a Simplex algorithm (Cacei and Cacheris, 1984); whether a two-exponential fit was better than a one-exponential fit was judged by an F test based on the residual sum of squares ($p < 0.01$).

Calculations of Passive Membrane Properties

The input resistance was determined from the slope of the linear part of the steady state current-voltage curve measured in normal Tyrode's solution containing 4 mM K (see Results). The membrane time constant was the time constant of a change in membrane potential of less than −10 mV induced at the resting potential by a rectangular hyperpolarizing pulse lasting 30 ms (current applied using the discontinuous current-clamp mode of the AxoClamp-2). The input capacitance was calculated using two methods. First, the input capacitance was obtained by dividing the membrane time constant by the input resistance (marked as input capacitance I in Table I). Second, voltage clamp was performed to step the membrane potential from −70 to −75 or −80 mV and the input capacitance was obtained by dividing the area under the capacitance transient by the voltage step (marked as input capacitance II in Table I). The surface area was calculated from the input capacitance, assuming that the specific membrane capacitance was 1 μF/cm^2. The specific membrane resistance was the product of the input resistance and the surface area.

The space constant (λ) was estimated by the equation:

$$\lambda = \sqrt{r_m/r_i} = \sqrt{(R_m/R_i) \times (a/2)},$$

assuming the cell to be a right cylinder with a diameter of a and assuming R_i to be 100–200 Ω·cm. When this calculation was carried out for two cells selected as most nearly approximating right cylinders, the space constant was 1.5–1.6 mm if R_i was 100 Ω·cm and 1.0–1.1 mm if R_i was 200 Ω·cm (Table I).

RESULTS

Characteristics of Canine Ventricular Myocytes: Passive Properties and Transmembrane Potentials

As previously reported (Hewett et al., 1983), ~50% of the isolated canine ventricular myocytes were rod-shaped and possessed clear, uniformly spaced striations. The surfaces were free of blebs (under a phase-contrast microscope at a magnification of 300). There were some pairs with cells coupled side by side or end to end. For apparent single cells, the width was 20–33 μm and the length was 110–140 μm.

Data are reported only for cells that maintained a resting membrane potential of greater than −80 mV. Spontaneous action potentials were sometimes seen just after impalement, when the membrane potential was less negative than the resting potential. For all cells described here, the spontaneous activity subsided as the resting potential became negative to −80 mV. Impalements with single microelectrodes could be maintained for ≥2 h when the cells were held near the resting potential. With holding potentials of −45 mV or more positive and clamp steps beyond the physiological range, the cells deteriorated more rapidly (1–1.5 h). With the suction pipettes, cells were suitable for data collection for 0.5–1 h.

The passive properties of these cells are summarized in Table I and compared with the properties reported for multicellular dog ventricular tissues (Sakamoto and Goto, 1970; Ikeda and Hiraoka, 1982). Two representative action potentials are illustrated in Fig. 1. The resting membrane potential was −84.2 ± 2.7 mV (n = 6) at 4 mM extracellular K, the maximal upstroke velocity of phase 0 ($\dot{V}_{max}$) was 284.8 ± 89.0 V/s (n = 6) (but for some cells, V_{max} was as high as 400 V/s, as shown in Fig. 1*A*), the action potential overshoot was +26.6 ± 10.3 mV (n = 5), and the plateau voltage, determined as the most positive voltage during phase 2 of the action potential, was −4.3 ± 13.1 mV (n = 6). At a cycle length of 9 s, the action potential duration at 50% repolarization was 226.5 ± 11.0 ms (n = 6), and at 90% repolarization, it was 292.3 ± 27.7 ms (n = 6). Although the cells were similar in terms of most action potential parameters, there appeared to be two subpopulations with respect to phase 1 repolarization. About half of the cells showed a prominent phase 1 and a notch between phase 1 and the plateau when driven at a cycle length >3 s (Fig. 1*A*). The rest showed slower repolarization during phase 1 and no notch, as shown in Fig. 1*B*. As will be shown below, this difference in action potential configuration is related to the presence or absence of a large transient outward current.

TABLE I

Passive Membrane Characteristics of Canine Ventricular Myocytes and Multicellular Canine Ventricular Tissues

Passive membrane characteristics	Isolated myocytes*	Multicellular tissues
Input resistance at RMP	61.2±18.0 MΩ	—
Membrane time constant at RMP	3.03±1.14 ms	3.0 ms,‡ 3.2 ms§
Input capacitance I	54.4±18.2 pF	—
Input capacitance II	80.4±16.2 pF	—
Surface area from input capacitance I	54.4±18.2 × 10^{-6} cm^2	—
Surface area from input capacitance II	80.4±16.2 × 10^{-6} cm^2	—
Specific membrane resistance	3.25±1.15 × 10^3 Ω·cm^2	3 × 10^3 Ω·cm^2‡ 5.3 × 10^3 Ω·cm^2§
Space constant	1.0–1.1 or 1.5–1.6 mm‖	0.8 mm‡, 1.2 mm§

* For all parameters (excluding space constant), $n = 6$ and mean ± SD is given.

‡ From Ikeda and Hiraoka (1982).

§ From Sakamoto and Goto (1970).

‖ The shorter values result from setting $R_i = 200$ Ω·cm; the longer values result from $R_i = 100$ Ω·cm.

Inward Rectifier Current

The inward rectifier current (I_{K1}) plays an important role in determining the resting membrane potential and the rate of repolarization during phase 3 of the action potential in isolated canine ventricular cells (Hewett et al., 1983). Fig. 2*A* shows the steady state *I-V* relationships for one cell exposed to several extracellular K concentrations ($[K]_o$) ranging from 1 to 16 mM. The steady state *I-V* relationships were obtained by applying a slow depolarizing ramp (1.4 mV/s) from −120 to +20 mV using the switched clamp and a microelectrode. Similar results were obtained in two other experiments in which we used the voltage clamp to step the membrane potential to different levels between −120 and +20 mV for 5–10 s. The steady state *I-V* curves displayed the following characteristics:

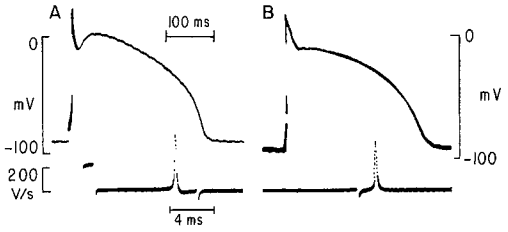

FIGURE 1. Records of transmembrane potentials (upper trace) and $\dot{V}_{max}$ (lower trace) from dog ventricular myocytes. In *A*, phase 1 repolarization is rapid and a notch separates phases 1 and 2; in *B*, repolarization during phase 1 is slow and the notch is absent. In *A*, the lower trace shows a calibration of 200 V/s for *dV/dt*. The stimulation cycle length was 9 s for both action potentials.

(*a*) prominent inward rectification, (*b*) a negative slope in a voltage range positive to the K equilibrium potential, and (*c*) a crossover of curves for different values of $[K]_o$. Also, a low concentration of Ba (0.1 mM) made the steady state *I-V* relationship almost linear (data not shown). At 1 and 2 mM $[K]_o$, the *I-V* curves crossed the voltage axis at three points, which indicates the existence of a second

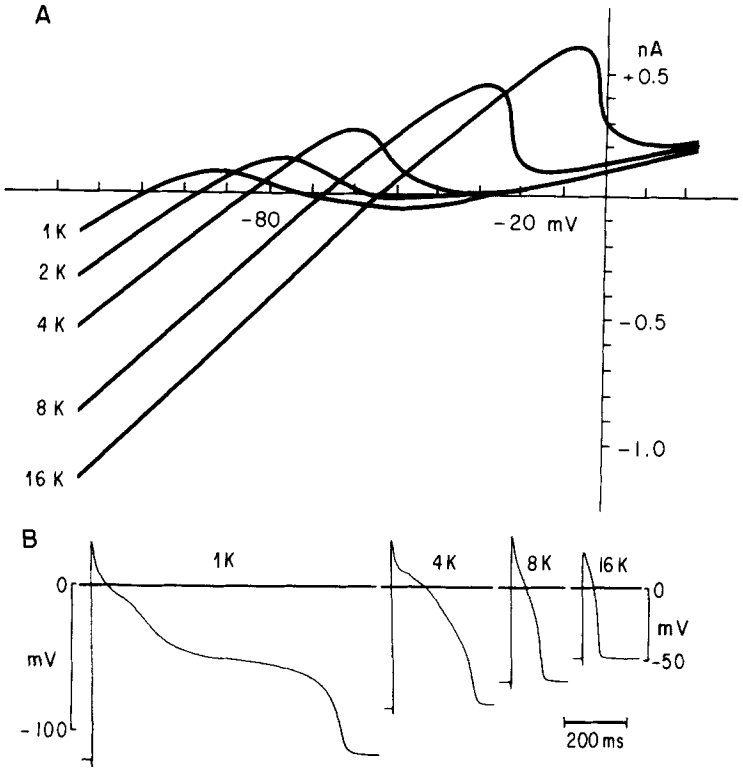

FIGURE 2. (*A*) Effects of $[K]_o$ on the steady state *I-V* relationship of a dog ventricular myocyte. (*B*) Effects of $[K]_o$ on action potential configuration of the same myocyte. $[K]_o$ was changed from 4 to 1, 2, 8, and 16 mM. Between exposure to each test solution, the superfusate was switched back to 4 mM $[K]_o$ until the resting membrane potential and the action potential configuration had recovered to control values. At 1 mM $[K]_o$, the resting membrane potential was −118 mV and the action potential either had a very long duration or the cell failed to repolarize fully and the membrane potential stayed at −40 to −50 mV. As $[K]_o$ was elevated, the resting membrane potential decreased and the action potential duration shortened. At 16 mM $[K]_o$, the action potential was not all-or-none: it was a graded slow response.

stable resting membrane potential (Gadsby and Cranefield, 1977). For the cell shown in Fig. 2, the *I-V* curve at 1 mM $[K]_o$ crossed the voltage axis with positive slopes at −110 and −20 mV, and the cell exhibited two stable resting membrane potentials: −118 and −40 to −50 mV; for 2 mM $[K]_o$, the two intersections were −98 and −24 mV, and the two observed resting membrane potentials were −98

and −27 mV. The input resistance of the cell decreased as $[K]_o$ increased: it was 100, 86.6, 75.8, 67.3, and 60.3 MΩ at 1, 2, 4, 8, and 16 mM $[K]_o$, respectively. A similar effect of changing $[K]_o$ on cell input resistance was observed in two other experiments.

Fig. 2*B* shows the action potential configurations at different extracellular K concentrations; these data were obtained from the same cell that provided the data in *A*. At low $[K]_o$ (1 mM), the action potential was very long. Sometimes, under these conditions, the cell failed to repolarize and the membrane potential stayed at −40 to −50 mV. A small hyperpolarizing current (<0.1 nA) could bring the membrane potential back to the high (more negative) level. At higher $[K]_o$ (8 or 16 mM), the action potential was very short. These effects of $[K]_o$ on action potential configuration can be explained by the effects of varying $[K]_o$ on I_{K1} as observed in the steady state *I-V* curves (Fig. 2*A*): a higher $[K]_o$ caused a larger outward current at voltages positive to the crossover voltage and this would speed repolarization.

Na Current

To study the response of the action potential upstroke to changes in membrane potential, we measured the maximum upstroke velocity of phase 0 ($\dot{V}_{max}$) while changing the membrane potential using the switched-clamp method with a single microelectrode. Fig. 3*A* illustrates the relationship between $\dot{V}_{max}$ and the membrane potential, summarized from data obtained in five cells. The membrane potential was clamped at selected holding potentials for >5 s and then, 0.3 ms after release of the clamp, the cell was stimulated by a depolarizing pulse 2 ms in duration. The strength of the current pulse was adjusted for each holding potential so that the latency between the end of the pulse and the moment of $\dot{V}_{max}$ was constant (~0.8 ms). The $\dot{V}_{max}$ values are normalized to the value obtained at a holding potential of −100 mV. In the five cells, the half-maximum potentials ranged from −62 to −51 mV, with an average of −55 ± 4 mV as indicated by the open circle and the horizontal bar in Fig. 3*A*. Superimposed on the data points are two curves calculated from the following equation:

$$\dot{V}_{max}(\%) = \left[\frac{1}{1 + \exp\left(\frac{V + 55}{K}\right)}\right] \times 100,$$

with $K = 2$ (solid curve) or 3 (dotted curve). It is clear that the $K = 2$ curve provides a reasonable fit to the data points.

Tetrodotoxin (TTX; 3.8 μM) decreased the action potential duration before it caused a significant decrease in overshoot or $\dot{V}_{max}$. This is shown in Fig. 3*B*, which compares the control action potential with that recorded after exposure for 0.5 min to TTX. With a decrease in $\dot{V}_{max}$ of only 10% (from 173.6 to 157 V/s) and an overshoot of +18.8 mV, there was probably no significant change in the activation of the transient outward current or Ca current, as indicated by the lack of change in phase 1 and the initial part of the plateau (for the voltage dependence of activation of the transient outward current and Ca current, see

below). However, the action potential duration (APD_{-60mV}) was shortened from 300 to 245 ms. The most likely cause of this shortening was partial blockade of a TTX-sensitive inward Na current that helps maintain the plateau (Coraboeuf et al., 1979; Gintant et al., 1984). After longer exposure to this concentration of TTX (right side of Fig. 3*B*, 3 min exposure), the overshoot and $\dot{V}_{max}$ decreased to 100 V/s and +8.6 mV, respectively. APD_{-60mV} decreased further to 215 ms. There was also a negative shift in the plateau voltage.

Transient Outward Current(s)

A transient outward current has long been recognized in sheep Purkinje fibers, which generate action potentials with a prominent phase 1 repolarization (Ken-

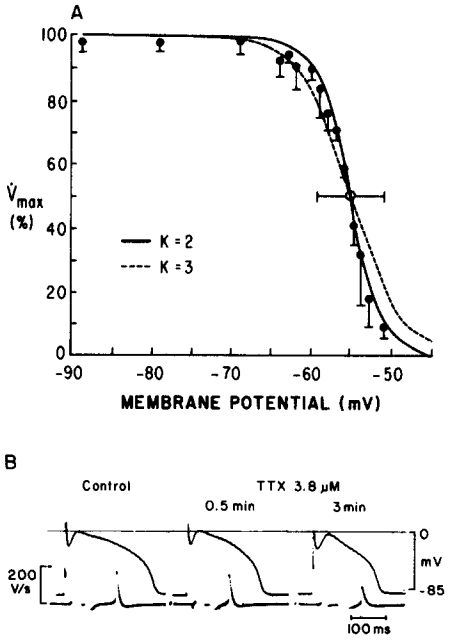

FIGURE 3. Contribution of the Na current to the action potential. (*A*) Effects of membrane potential on $\dot{V}_{max}$ of phase 0. Data show the means ± SD for five cells. The $\dot{V}_{max}$ values for each cell were normalized to the value obtained at a holding potential of −100 mV, and the half-maximum voltages were determined. The open circle and horizontal bar represent the mean half-maximum voltage for the five cells, −55 ± 4 mV. The recorded transmembrane voltages for each cell were normalized by taking the half-maximum voltage to be −55 mV. The dots show the normalized mean values of $\dot{V}_{max}$ at the normalized voltages. The two curves represent the calculated values of $\dot{V}_{max}$ according to the Boltzmann function with the half-maximum voltage of −55 mV and the slope factor (K) of 2 (solid curve) or 3 (dashed curve). The $\dot{V}_{max}$ value used for normalization ranged from 202 to 304 V/s (255.4 ± 49.7 V/s; mean ± SD, n = 5). (*B*) Effects of TTX (3.8 μM) on the action potential configuration (upper trace) and dV/dt (lower trace). The action potentials before and 0.5 and 3 min after exposure to TTX are shown. The cell was driven at a cycle length of 5 s.

yon and Gibbons, 1979). More recently, two components of the transient outward current have been identified: one is blocked by 4-aminopyridine (4-AP) and another is activated by intracellular Ca (Siegelbaum and Tsien, 1980; Coraboeuf and Carmeliet, 1982). In about half of the canine ventricular cells, we found two components of the transient outward current. In cells generating action potentials with fast repolarization during phase 1 and a prominent notch between phase 1 and the plateau, voltage steps from holding potentials negative to −60 mV to

levels positive to −20 mV activated a large transient outward current. Two examples are illustrated in Fig. 4. Panels *A* and *B* show current traces recorded from two different cells, both exhibiting fast phase 1 repolarization and a notch. The currents result from voltage steps from −90 (upper) or −70 (lower) to +40 mV. The current reached a peak within 5–10 ms and then decayed during maintained depolarization. 4-AP (2 mM) abolished most of this outward current and revealed a slower and smaller component. This 4-AP–resistant current component had a time to peak of 15 ms, and an amplitude only 10–20% of the transient outward current under the control conditions. Mn (2 mM, Fig. 4*A*) or caffeine (10 mM, Fig. 4*B*) abolished the 4-AP–resistant outward current. Ryanodine, an agent that specifically blocks Ca release from the sarcoplasmic reticulum (Sutko and Kenyon, 1983), abolished the 4-AP–resistant outward current (data not shown; Tseng, G.-N., and B. F. Hoffman, manuscript submitted for publication). The inhibitory effects of 4-AP, Mn, and caffeine were reversible. We

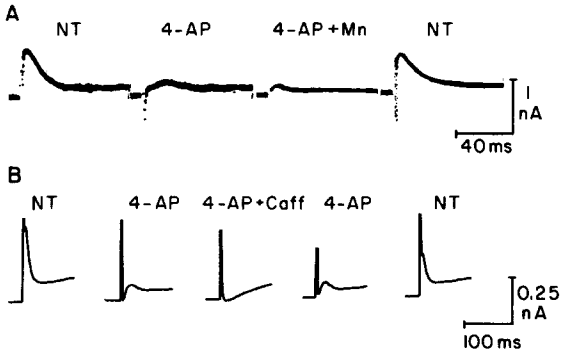

FIGURE 4. Two components of the transient outward current. Voltage clamp was performed with the switched-clamp method and the current traces were recorded with Polaroid film (*A*) or a chart recorder (*B*). From a holding potential of −90 mV (*A*) or −70 mV (*B*), the membrane potential was clamped to +40 mV at intervals of 7 s. Normal Tyrode's solution (NT), 2 mM 4-AP, 2 mM Mn, and 10 mM caffeine were used. See text for description.

will refer to the component blocked by 4-AP as I_{to1} and the component blocked by Mn or caffeine as I_{to2}.

Fig. 5 shows the relationship between the transient outward current and the notch and phase 1 of the action potential. The voltage clamp was performed with the switched-clamp method with a single microelectrode. Panel *A* shows that 4-AP (2 mM) slowed phase 1 repolarization and abolished the notch. During voltage clamp, the same voltage-clamp protocol that activated a large and fast transient outward current under control conditions no longer did so: only the smaller and slower 4-AP–resistant transient outward current remained. Panel *B* shows that both the notch of the action potential and the transient outward current were interval dependent. At a short coupling interval between action potentials or clamp steps (upper row), the notch was absent from the second action potential and the transient outward current was absent during the second

pulse. As the interval was prolonged (lower row), both recovered. Thus, the transient outward current, I_{to1}, causes the rapid phase 1 repolarization and notch when these are present in the action potentials of canine ventricular cells.

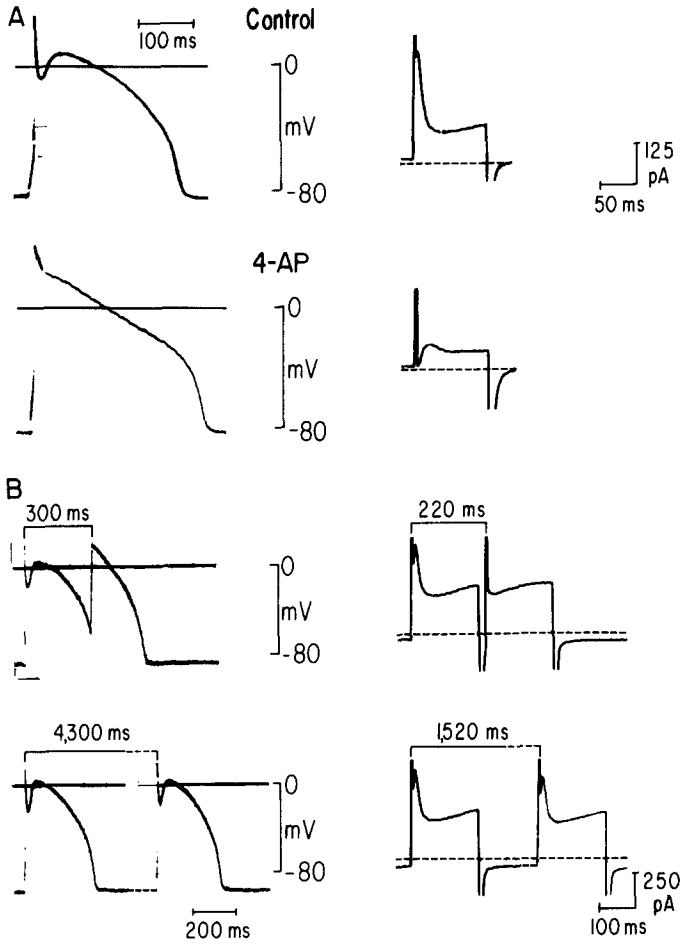

FIGURE 5. Records showing relationships between rapid repolarization during phase 1, the notch, and the transient outward currents. *A* shows, on the left, a control action potential from a myocyte stimulated at a cycle length of 9 s and the loss of rapid phase 1 repolarization and the notch during exposure to 2 mM 4-AP. On the right are traces from the chart recorder showing the currents elicited by voltage-clamp steps from −90 to +20 mV. The large, rapid transient outward current seen under control conditions (I_{to1} and I_{to2}) is replaced by a smaller, slower outward current (I_{to2}) during exposure to 4-AP. *B* shows the effect of the interstimulus interval on the action potential and outward currents. A premature action potential elicited 300 ms after the driven response shows no rapid repolarization or notch, whereas one elicited after an interval of 4,300 ms shows full recovery of both. A voltage-clamp step from −70 to +20 mV elicits no transient outward currents at an interval of 220 ms and nearly full recovery of the transient outward currents at an interval of 1,520 ms. A switched voltage-clamp method was employed; the dashed lines show zero current.

However, the recovery time courses of the notch and the transient outward current differed: the notch recovered with a halftime of 1,300 ms (at a resting membrane potential of −90 mV) and the transient outward current recovered with a halftime of 250 ms (at a holding potential of −70 mV). This discrepancy is probably due to the involvement of not only the transient outward current but also the Ca current in the formation of the notch (see Discussion). For cells having slower repolarization during phase 1 and no notch, only I_{to2} could be demonstrated by voltage clamp. The contribution of I_{to1} to phase 1 of repolarization can be depicted in a more quantitative manner: for the cell shown in Fig. 4*A*, with a peak amplitude of I_{to1} of 0.7 nA and an input capacitance of 55 pF, the calculated rate of repolarization during phase 1 was 13 V/s. This is very close to the experimentally observed value of 12 V/s. I_{to2} does not make an important contribution to phase 1 repolarization or the notch, as can be seen in Fig. 5*A*. After the addition of 4-AP, even though I_{to2} was present, phase 1 repolarization was markedly slowed and there was no notch.

Ca Current

The voltage-clamp experiments on the Ca current were done by the continuous-clamp method with a suction pipette. The pipette solution contained 10 mM EGTA and 5 mM ATP to prevent appreciable "rundown" of the Ca channels for ≥30 min. Contamination by I_{to2}, whose activation depended on the intracellular Ca level (Siegelbaum and Tsien, 1980), was eliminated by the strong Ca buffering of 10 mM EGTA in the pipette solution. Contamination by Na or K currents was eliminated by one of two methods: (*a*) a holding potential of −45 mV or less negative was used to inactivate both the Na current and the transient outward current, or (*b*) an Na- and K-free external solution and Cs-containing pipette solution removed the charge carriers for Na and K currents. Fig. 6 shows the results obtained with the first method. Panel *A* shows the superimposed original traces of Ca current elicited by depolarization to selected voltages. As is the case for other single cardiac cells (Isenberg and Klockner, 1982*b*), activation of the Ca current in canine ventricular cells was fast (time to peak, ≤10 ms). The activation threshold for the Ca current was between −40 and −30 mV. At −35 mV, the Ca current showed no appreciable or very slow inactivation. At more positive voltages, the Ca current showed inactivation, which first increased and then decreased in rate as the membrane voltage became more positive. Fig. 6*B* shows the *I-V* relationships of the Ca current. At 2 mM $[Ca]_o$, the peak Ca current reached a maximum between −10 and 0 mV and showed an apparent reversal between +50 and +60 mV. In the voltage range from −25 to +35 mV, the current was still inward 200 ms after the start of the depolarizing clamp step. Similar results were obtained in four other experiments.

Fig. 6*C* shows the results from an experiment on another cell. At a holding voltage of −30 mV, the Ca channel blocker nisoldipine could abolish the peak Ca current and shift the late current in the outward direction, which suggests that there is a component of slowly inactivating or noninactivating Ca current in the late current. Fig. 7 shows the voltage-dependent activation and inactivation of the Ca current. The Na and K currents were largely eliminated by using the Na- and K-free external solution and the Cs-containing pipette solution. In the

experiment shown in Fig. 7, $[Ca]_o$ was 5 mM and there was ryanodine (1 μM) in the external solution to suppress intracellular Ca transients caused by Ca release from the sarcoplasmic reticulum. Step depolarizations to −30 mV or more positive voltages activated a Ca current similar to that seen in Fig. 6; as the voltage was made more positive, the peak inward current increased in amplitude,

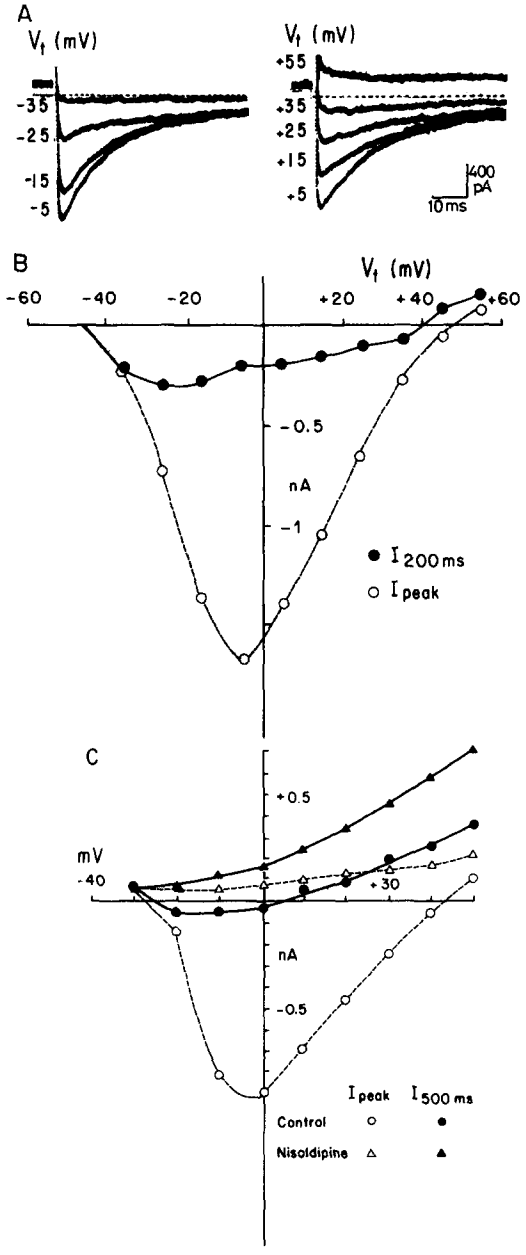

FIGURE 6.

reached a maximum at +5 to +10 mV, and then decreased, showing an apparent reversal between +55 and +65 mV. At −30 to −25 mV, there was very little inactivation; at more positive voltages, the inactivation rate first increased and then decreased. Current remained inward 300 ms after the start of the depolarization in a voltage range from −30 to +30 mV (Fig. 7, *A* and *B*). Calculation of the Ca current activation curve (curve *d*) from the peak current amplitude at each voltage and the apparent reversal potential (+60 mV) gave a sigmoidal curve that had a threshold between −30 and −20 mV and reached a plateau between +10 and +20 mV (Fig. 7*D*). Fig. 7, *C* and *D*, also illustrates the voltage-dependent inactivation of the Ca current. The upper panel of Fig. 7*C* shows the voltage-clamp protocol: the cell was clamped to different conditioning voltages (V_c) for 500 ms and then to the test voltage of +20 mV for 300 ms. The amplitude of the Ca current at the test voltage (Fig. 7*C*, lower panel) was measured and normalized with respect to the maximum Ca current obtained at conditioning voltages negative to −55 mV. The inactivation curve (curve *f*) was then constructed and is shown in Fig. 7*D*. The inactivation curve is sigmoidal, extending over a voltage range from −45 to 0 mV, with a half-maximum voltage at −20 mV. Similar observations were obtained in four other cells. There was an overlap between the activation and inactivation curves, with the maximum overlap occurring at about −15 mV.

Fig. 8 illustrates some of the kinetic properties of the Ca current. At certain voltages, the time course of decay of the Ca current can be described by the sum of two exponential components (Fig. 8*A*). However, at voltages negative to −20 mV and positive to +30 mV, the time course of decay was not well fitted by two exponentials. The time course of Ca current decay was therefore described by peeling off the slow current change occurring after 125 ms and fitting the initial 50-ms change with a single exponential. The resulting time constants of Ca current decay at various potentials in three different experiments are illustrated in Fig. 8*B*. The decay time constant decreased as the voltage changed from −40 to 0 mV and increased at more positive voltages. The Ca current recovered from inactivation with a voltage-dependent time course. About 90% of the recovery could be described by a single exponential with a time constant of 60–70 ms at −50 mV and ~120 ms at −40 mV (data not shown).

FIGURE 6. (*opposite*) Voltage-dependent activation of Ca current and the effects of nisoldipine. Voltage clamp was performed with the continuous-clamp method. The external solution was normal Tyrode's solution (2 mM Ca) and the pipette was filled with K-containing solution. Contamination by Na and I_{to1} was avoided by using a holding potential of −45 mV (*A* and *B*) or −30 mV (*C*). I_{to2} was suppressed by 10 mM EGTA in the pipette solution. (*A*) Superimposed original current traces with the test (depolarization) voltages (V_t) marked to the left of the traces. The dashed line represents the zero-current level. (*B*) *I-V* relationships of the peak inward current (open circles) and of the current 200 ms after the start of the depolarization (filled circles) from the same experiment as in *A*. (*C*) Current recording obtained from another cell. Nisoldipine (1 μM) abolished the peak inward current and shifted the current level 500 ms after the start of depolarization in the outward direction.

Delayed Rectifier Current

It is usually thought that in the ventricular myocardium, particularly from dogs and sheep, the delayed rectifier current (I_x) is very small or nonexistent and makes a negligible contribution to repolarization (Noble, 1980). However, in

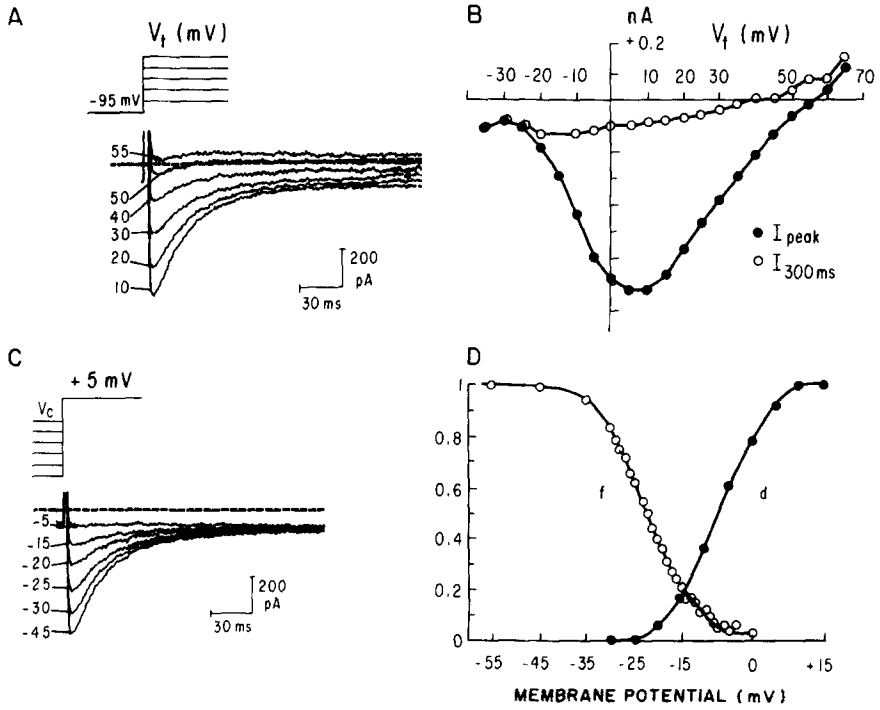

FIGURE 7. Voltage-dependent activation and inactivation of the Ca current. Voltage clamp was performed with the continuous-clamp method. Contamination by Na and K currents was avoided by using the Cs-containing pipette solution and Na- and K-free external solution. The external solution contained 5 mM Ca and 1 μM ryanodine. The holding potential was −95 mV. (*A*) The upper panel shows the voltage-clamp protocol for studying activation of the Ca current. The lower panel shows the superimposed original current traces with the test voltage (V_t) marked for each. (*B*) *I-V* relationships showing the peak inward current (filled circles) and the current 300 ms after the start of the test pulse (open circles). (*C*) The upper panel shows the voltage-clamp protocol to study inactivation of the Ca current. The lower panel shows superimposed original current traces with the conditioning voltage marked (V_c) for each. (*D*) Activation (curve *d*) and inactivation (curve *f*) curves of the Ca current. The calculation of *d* and *f* is presented in the text. The dashed lines in *A* and *C* represent the zero-current level.

canine ventricular myocytes, I_x is clearly present and therefore probably plays a role in repolarization.

To study the delayed rectifier current, voltage clamp was performed with the continuous-clamp method using a suction pipette filled with the K-containing solution. Interference from the Na current and the transient outward current

was reduced by using holding voltages between −50 and −30 mV. Since the voltage-clamp protocols used to study the delayed rectifier current required strong depolarizing pulses of long duration, there might have been changes in the intracellular Ca or Na concentrations. The use of the K-containing pipette solution containing 10 mM EGTA and no Na was intended to limit interference from current changes depending on intracellular Ca, e.g., oscillatory current and

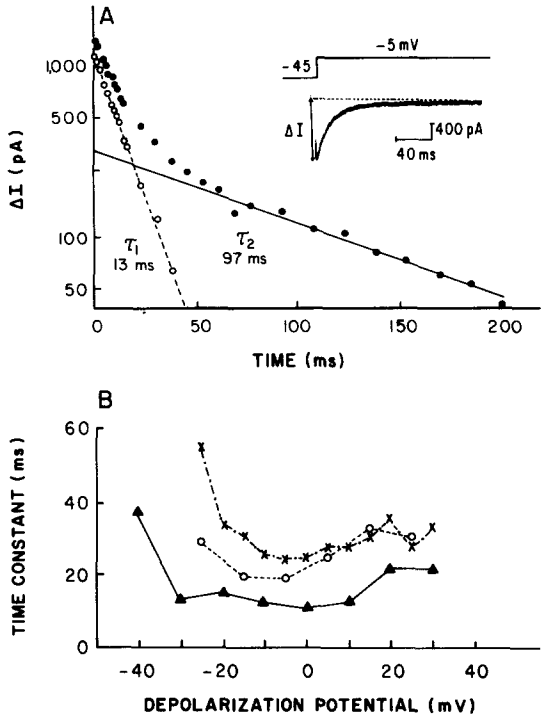

FIGURE 8. Kinetic properties of the Ca current. Voltage clamp was performed with the continuous-clamp method with normal Tyrode's solution outside and K-aspartate solution inside. The inset in *A* shows one original current trace. The difference between the inward current level and the steady current level was measured and plotted against time in the semilog plot. Inactivation of I_{Ca} can be fitted by the sum of two exponentials, the time constant of the fast component (τ_1) being 13 ms and that of the slow component (τ_2) being 97 ms. *B* shows the U-shaped dependence of the time constant for I_{Ca} inactivation on voltage in three cells. The time constants were obtained by fitting the initial 50-ms change in I_{Ca} with a single exponential after peeling off the slow current changes occurring after 125 ms.

Na/Ca exchanger current, and from current changes depending on intracellular Na, e.g., Na pump current. To preclude any remaining interference from the Ca current, in some experiments, the Ca current was reduced by adding Mn (2 mM) or nisoldipine (1 μM) to the external solution.

To study the activation of I_x, we applied depolarizing steps of 0.5–5 s from a holding potential of −50 to −30 mV and measured the amplitudes of the tail

currents upon return to the holding potential. Fig. 9*A* shows the voltage-dependent activation of I_x, revealed as the outward tail currents. In this experiment, the holding potential was −50 mV and the outward tail current appeared after a depolarizing step positive to −25 mV. The tail current was measured as the difference between the outward peak and the steady current level after the decay of the tail current. The delayed rectifier current activation curve was then constructed by dividing the tail current amplitude after each depolarizing step by that recorded after depolarization to +55 mV and plotting the percentage vs. depolarization voltage. The I_x activation curve summarized from four experiments is plotted in Fig. 9*B*. The activation of the delayed rectifier displayed a

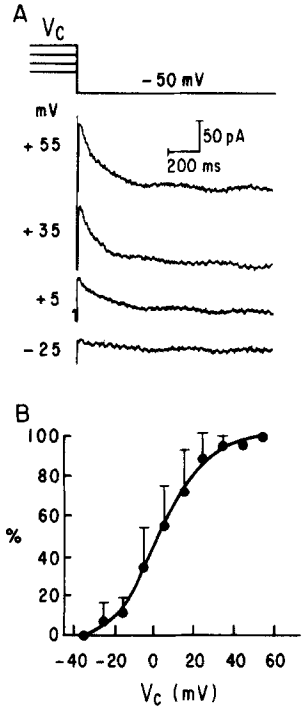

FIGURE 9. Voltage-dependent activation of the delayed rectifier current. Voltage clamp was performed using the continuous-clamp method with normal Tyrode's solution outside and K-aspartate solution inside. *A* shows the outward current tails recorded at −50 mV after depolarization for 500 ms to different conditioning voltages (V_c), marked on the left. The tail current amplitude was measured as the difference between the outward peak and the steady current after decay of the tail current (holding current, +100 pA). *B* shows tail current amplitudes as a function of conditioning voltages; values were normalized with respect to the amplitude of tail current elicited by depolarization to +55 mV. The filled circles and bars are means ± SD; $n = 4$.

sigmoidal voltage dependence, with a threshold between −40 and −30 mV and a plateau at about +55 mV.

Fig. 10 shows the envelope test of the delayed rectifier current. The upper and middle traces are the current activated during depolarization and the superimposed tail currents after depolarizations of various durations. The lower plot is the normalized difference current vs. the duration of depolarization. The difference current is either the difference between the amplitude of the activating current and the current at 10 s depolarization, or between the tail current amplitude after each depolarization and the tail current amplitude after a 10-s depolarization. Both the activating current and the growth of the tail current

can be fitted well by double-exponential time courses, and the percentage contribution to the total current and the time constant of each process are shown in the inset. It is clear that the percentages of fast and slow processes are similar for the activating current and the tail currents; the fast time constants also are similar. There is some difference in the slow time constants, the reason for which is not clear.

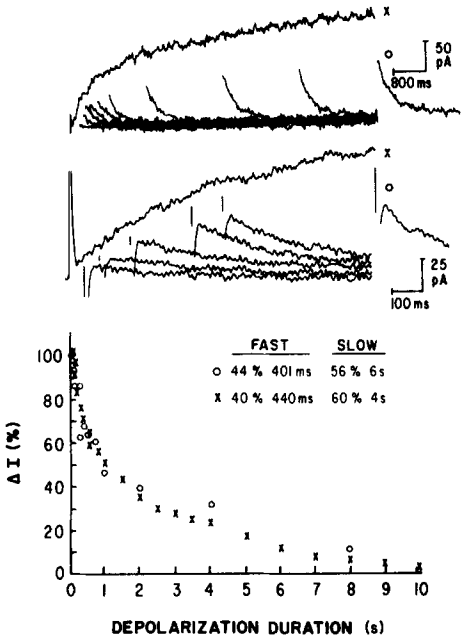

FIGURE 10. Envelope test of the delayed rectifier current. The current was recorded with the continuous-clamp method using a suction pipette filled with the K-containing solution. External solution was normal Tyrode's solution containing nisoldipine (1 μM). The holding potential was −30 mV and depolarizing pulses to +50 mV for various durations (30 ms to 10 s) were applied every 20 s. The upper panel shows the current activated during depolarization for 8 s (the trace marked by an ×) and superimposed tail currents after depolarization for various durations (traces marked by an open circle). The initial part of the currents (up to 1 s) is shown with expanded time and current scales in the middle panel. The lower plot shows the time courses of current changes. The ordinate is percent of difference current [ΔI(%)]: for current activated during depolarization (×), the differences between currents after depolarizations of various durations and the current after a 10-s depolarization were measured and normalized to the current at 10 s; for the tail currents after depolarizations of various durations (○), the differences in the tail current amplitudes and that after a 10-s depolarization were measured and normalized to the tail current amplitude after depolarization for 10 s. The abscissa is the duration of depolarization. The time courses of both the current activation during depolarization and tail current growth after depolarizations of various durations are well fitted by a double-exponential process; the percent and time constant of each process for each current are shown in the inset.

Fig. 11 shows the activation and deactivation time courses of the delayed rectifier current. Both activation and deactivation processes could be better described by a double-exponential time course than by a single-exponential time course. Fig. 12 depicts the voltage dependence of the kinetics of the delayed rectifier current. The initial parts of deactivation and activation are shown in *A* and *B*, respectively. It is clear that both time courses were accelerated at more

negative (*A*) and more positive (*B*) voltages. Panel *C* shows the fast time constants of deactivation (filled circles) and activation (open circles) at different voltages. The relationship between time constants and voltage is bell-shaped. Similar results (bell-shaped curves) were obtained in five other cells.

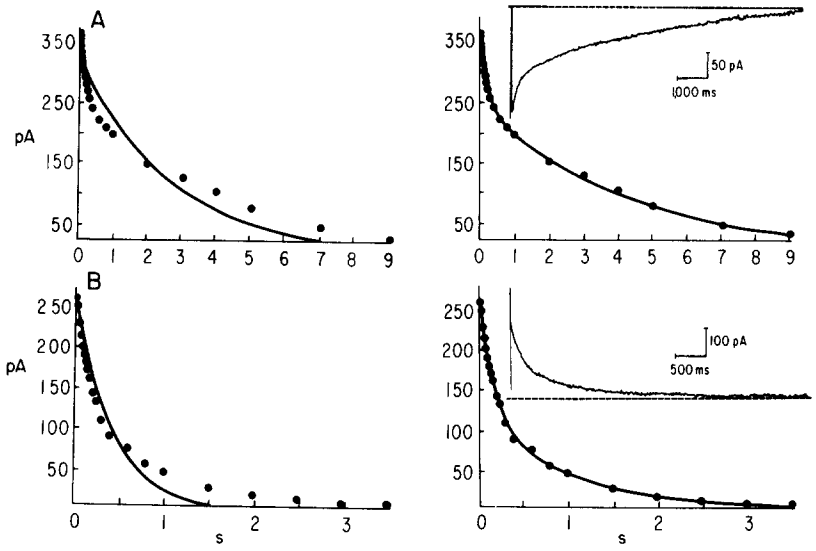

FIGURE 11. Double-exponential time courses of activation and deactivation of the delayed rectifier current. Voltage clamp was done using the continuous-clamp method and the suction pipette was filled with the K-containing pipette solution. The external solution contained TTX (16 μM) and nisoldipine (1 μM). The holding potential was −30 mV. (*A*) The inset of the right-hand panel is an original trace of I_x activation elicited by a depolarization step from the holding potential to +70 mV for 10 s. The differences between current levels at various times after the initial 7 ms after the start of depolarization and that at 10 s (marked by the interrupted line) were measured and plotted in both panels. Superimposed upon the current measurements is a curve calculated from a single-exponential (left) or a double-exponential (right) process. The *F* test, based on the residual sum of squares, indicated that a double-exponential provided a better fit ($p < 0.01$). (*B*) The inset of the right-hand panel is an original trace of I_x deactivation elicited by a repolarization step to −10 mV after a depolarization pulse to +30 mV for 5 s. The differences between current levels at various times after the initial 7 ms after the start of repolarization and that at 5 s (marked by the dashed line) were measured and plotted in both panels. The curves were calculated from a single-exponential (left) or a double-exponential (right) process. The *F* test indicated that a double-exponential provided a better fit ($p < 0.01$).

Fig. 13 shows the *I-V* relationship and reversal potential of the delayed rectifier current summarized from eight experiments. In each experiment, the cell was depolarized to +30 mV for 5 s and then repolarized to different voltages for 5 s. The amplitude of tail current was measured during each step repolarization and normalized with respect to the maximum outward tail current. The shapes

of the *I-V* curves and the estimated reversal potentials were similar in the different experiments. The summarized *I-V* relationship shows inward rectification at −20 mV. The average reversal potential was −71.3 ± 3.5 mV.

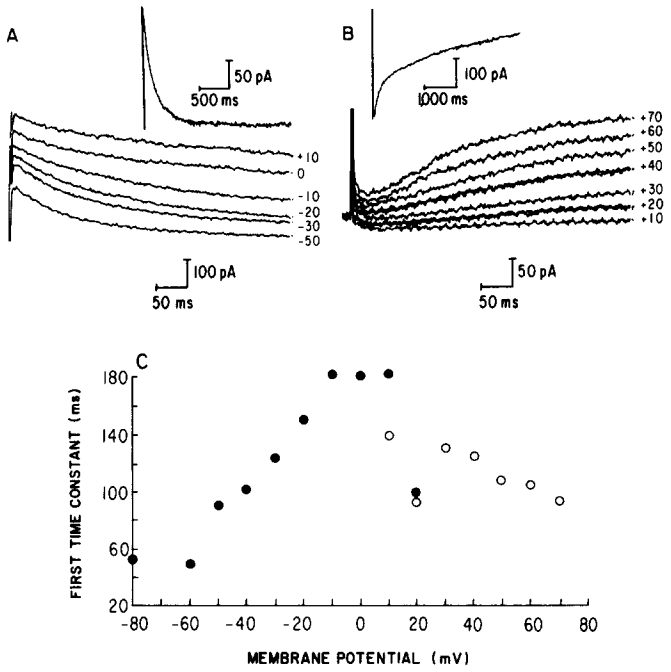

FIGURE 12. Voltage dependence of the kinetics of activation and deactivation of the delayed rectifier current. Voltage clamp was performed with the continuous-clamp method and a suction pipette filled with K-containing pipette solution. The external solution contained TTX (16 μM) and nisoldipine (1 μM). The holding potential was −30 mV. For activation time courses (*B* and open circles in *C*), the membrane was depolarized to various voltages for 5 s every 15 s and the time course of current change during depolarization was measured. For deactivation time courses (*A* and filled circles in panel *C*), the voltage was stepped to +30 mV for 5 s and then repolarized to various voltages for 5 s every 15 s, and the time course of current change after repolarization was measured. The insets of *A* and *B* illustrate the representative time courses of deactivation (tail current at −30 mV) and activation (current at +70 mV). The initial parts of the deactivation and activation at various voltages are shown in *A* and *B*, respectively, with the voltages marked to the right of the traces. The time constants of these initial exponential processes (first time constants) are plotted against voltage in *C*, with open circles for activation and filled circles for deactivation processes.

The contributions of I_{Ca} to the action potential plateau and of I_x to repolarization are best illustrated by comparing the action potential configurations before and after the addition of isoproterenol, which has been shown to increase the amplitude of both I_{Ca} and I_x in cardiac tissues (Kass et al., 1982). The comparison is illustrated in Fig. 14. Isoproterenol (1 μM) shifted the plateau voltage from 0

to +23 mV and shortened the action potential: APD_{-60mV} decreased from 260 to 160 ms (Fig. 14, top left). During voltage clamp using the switched-clamp method on the same cell (Fig. 14, top right), isoproterenol induced a 5-fold increase in the amplitude of I_{Ca} and a 3.5-fold increase in I_x. These measurements are approximate because the switched-clamp method was too slow to accurately indicate the peak value of I_{Ca} and the oscillatory current was superimposed on the I_x tail. The bottom panel of Fig. 14 shows the effect of nisoldipine on the changes in the action potential configuration caused by isoproterenol. Nisoldipine

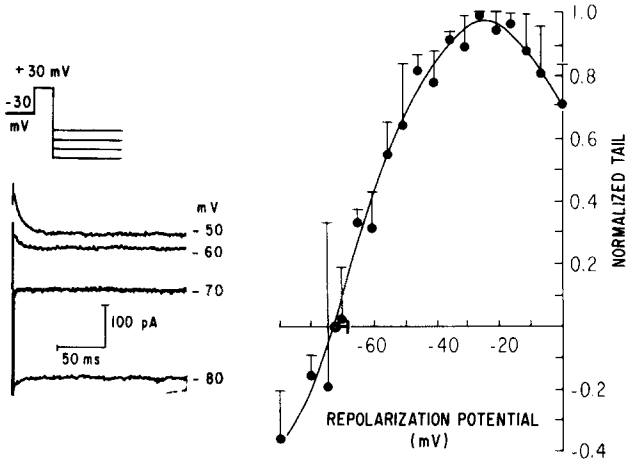

FIGURE 13. *I-V* relationship and reversal potential of the delayed rectifier current. (*Left*) The voltage-clamp protocol and some superimposed original current traces from a representative experiment. Voltage clamp was performed with the continuous-clamp method using a suction pipette filled with K-containing pipette solution. The external solution contained TTX (16 μM) and nisoldipine (1 μM). The holding potential was −30 mV and a 5-s depolarization step to +30 mV, followed by a 5-s repolarization step to different voltages, was applied every 15 s. The repolarization voltages are marked on the right of the current traces. (*Right*) The *I-V* relationship of I_x summarized from eight experiments. In each experiment, the tail currents were measured and normalized with respect to the maximum outward tail current, which occurred between −15 and −25 mV. The normalized tail currents from different experiments were pooled and shown. The circles and bars are means ± SD. The smooth curve was drawn by eye. Reversal potentials estimated in different experiments were also pooled and are shown as the open circle and horizontal bar: −71.3 ± 3.5 mV.

abolished the change in plateau voltage caused by isoproterenol, but the shortening of action potential persisted. This indicates that the decrease in the action potential duration resulted largely from the increase in I_x.

DISCUSSION

Passive Properties and Action Potential Characteristics

The passive properties of dog ventricular myocytes reported here are similar to those described for isolated preparations of dog ventricular tissue as seen in

Table I (Sakamoto and Goto, 1970; Ikeda and Hiraoka, 1982). The myocytes demonstrated an action potential plateau somewhat less positive and an action potential duration longer than the values reported for the transmembrane potential recorded from surface cell layers of multicellular ventricular tissue (Hewett et al., 1983; Hoffman and Cranefield, 1960). This discrepancy may be due to the fact that our ventricular myocytes were isolated from the deep myocardium, where the action potential has a lower plateau voltage and longer duration than in the surface myocardium (Solberg et al., 1974; see also Watanabe et al., 1985).

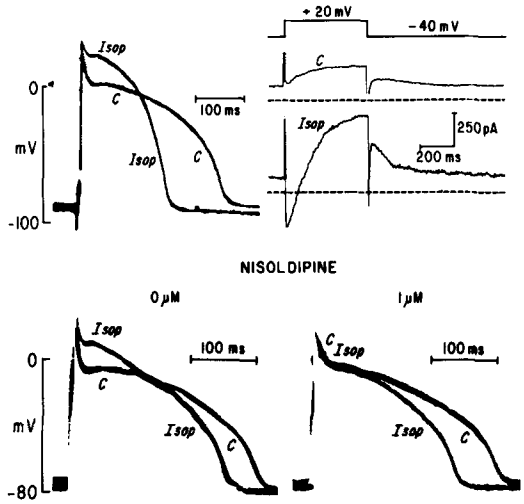

FIGURE 14. The contribution of the Ca current to the action potential plateau, and of the delayed rectifier current to repolarization. (*Top*) The left-hand panel shows superimposed action potentials recorded before (*C*) and after exposure to 1 μM isoproterenol (*Isop*). Isoproterenol caused a positive shift of the plateau voltage, a shortened phase 2, and accelerated phase 3 repolarization. The right-hand panel shows the current response to a step to +20 mV from a holding potential of −40 mV. Voltage clamp was performed with the switched-clamp method and the current was recorded on a chart recorder. Isoproterenol increased the amplitudes of both the Ca current and the delayed rectifier current. Note the increase in the outward tail current caused by isoproterenol. The dotted lines represent the zero-current level. (*Bottom*) Both panels show superimposed action potentials recorded before (*C*) and after exposure to 1 μM isoproterenol (*Isop*), the left in the absence and the right in the presence of 1 μM nisoldipine. The stimulation cycle length was 1 s. In the presence of nisoldipine, isoproterenol still shortened the action potential without elevating the plateau voltage.

Inward Rectifier Current

The steady state *I-V* curves of dog ventricular myocytes show inward rectification with a negative slope region positive to the K equilibrium potential and a crossover of curves obtained at different values of $[K]_o$. Ba made the steady state *I-V* curve nearly linear and an increase in $[K]_o$ decreased the input resistance at

the resting potential. These findings are similar to those reported for intact ventricular tissue of dog (Beeler and Reuter, 1970) and other species (Trautwein, 1973), and for isolated ventricular cells of other species (Isenberg and Klockner, 1982*a*; Sakmann and Trube, 1984). The findings suggest that the characteristics of the steady state *I-V* curves depend largely on the inward rectifier current, I_{K1} (Sakmann and Trube, 1984). The dominant role of I_{K1} in determining the resting potential and controlling repolarization is clearly shown in Fig. 2. An increase in $[K]_o$ shifted the resting membrane potential in a positive direction and shortened the action potential by augmenting the net outward current at plateau voltages. However, we cannot exclude the possibility that depolarization will decrease the Na "window" current, which helps maintain the plateau (see below).

Na Current

The maximum upstroke velocity of phase 0 of the action potential is affected by the membrane voltage owing to the change in Na channel inactivation caused by altering membrane voltage (Weidmann, 1955). We used the voltage clamp to shift the membrane voltage to a given level for 5–10 s to cause steady state inactivation of Na channels (Carmeliet and Vereecke, 1979) and then elicited an action potential after terminating the clamp. By adjusting the strength of the stimulus used to elicit responses after clamping at various voltages, the latency between the end of the stimulus and the moment of the $\dot{V}_{max}$ stayed relatively constant at 0.8 ms. The resulting relationship between $\dot{V}_{max}$ and membrane voltage was quite consistent among different myocytes and can be described by the Boltzmann distribution function with half-maximum voltage ($V_{0.5}$) at −55 mV and a slope factor (K) of ~2 mV.

Whether or not the $\dot{V}_{max}$ is a linear measure of g_{Na} is an unsettled issue (Grant et al., 1984; I. Cohen et al., 1981). We do not mean to imply that our data for $\dot{V}_{max}$ measure Na channel inactivation. We believe that $\dot{V}_{max}$ is more useful than g_{Na} in predicting the response of the action potential upstroke to changes in membrane potential. Our data show that dog ventricular muscle and Purkinje fibers differ in the dependence of $\dot{V}_{max}$ on membrane potential: dog ventricular muscle can generate a fast upstroke in the voltage range from −60 to −55 mV, whereas Purkinje fibers cannot; at voltages positive to −55 mV, the ability of ventricular muscle to generate a fast upstroke abruptly decreases (Gintant et al., 1983; Sheets et al., 1983). These differences should be taken into account when considering changes in impulse conduction in a setting such as ischemia, when the membrane potential is decreasing.

There is a TTX-sensitive Na window current (Atwell et al., 1979) or slowly inactivating Na current (Gintant et al., 1984) in cardiac tissues. This current may contribute an inward current component in the voltage range between −70 and +5 mV (Atwell et al., 1979; Gintant et al., 1984) and thus help maintain the plateau. In dog ventricular myocytes, TTX shortened the action potential, without significantly decreasing $\dot{V}_{max}$, the overshoot, or the early plateau voltage. The most likely explanation for these effects of TTX is the inhibition of a TTX-sensitive Na current. A similar finding for dog ventricular muscle was obtained by Coraboeuf et al. (1979).

Transient Outward Current

As shown in Fig. 1, the action potentials of roughly half of the myocytes showed fast repolarization during phase 1 and a prominent notch between phase 1 and the plateau; the other myocytes showed slow repolarization during phase 1 and had no notch. The cells having a fast phase 1 and a notch were not likely to be contaminating Purkinje cells, because, during disaggregation, both the endocardial and epicardial tissues were removed and only midwall myocardium was used. The absence of the notch from the action potential of about half of the myocytes was not due to an excessively short cycle length or an inappropriately low resting potential. Differences in the prominence of phase 1 and the notch have been reported for action potentials recorded from different areas of the dog ventricle: ventricular tissue close to the epicardium displays a more prominent phase 1 and notch than that close to the endocardium (Moore et al., 1965). Recently, a pronounced phase 1 and a notch between phase 1 and plateau were observed in subepicardial, but not subendocardial, dog ventricular muscle (Litovsky and Antzelevitch, 1986). In the cells displaying a prominent notch and fast repolarization during phase 1, voltage clamp revealed a large transient outward current. 4-AP abolished most of this current (I_{to1}), leaving only a small and slow component (I_{to2}) that was blocked by 2 mM Mn or 10 mM caffeine and thus was probably induced by intracellular Ca. This is also supported by the observation of an inhibitory effect on I_{to2} of ryanodine (Tseng, G.-N., and B. F. Hoffman, manuscript submitted for publication). As shown in Fig. 5, the larger component, I_{to1}, is largely responsible for the phase 1 repolarization and the notch. A transient outward current was observed in an early voltage-clamp study on dog ventricular myocardium (Beeler and Reuter, 1970).

The transient outward current has been well characterized in sheep Purkinje fibers (Kenyon and Gibbons, 1979), which demonstrate rapid phase 1 repolarization and a notch in the action potential. More recently, a transient outward current was also observed in other multicellular cardiac preparations (Siegelbaum and Tsien, 1980; Kukushkin et al., 1983) and isolated cardiac myocytes (Giles and van Ginneken, 1985; Nakayama and Irisawa, 1985; Josephson et al., 1984*b*). Moreover, two components of the transient outward current have been identified: one is blocked by 4-AP and the other is activated by intracellular Ca (Siegelbaum and Tsien, 1980; Coraboeuf and Carmeliet, 1982).

Although I_{to1} decays rapidly, it can probably affect the action potential duration by changing the voltage of the initial part of the plateau and therefore the activation and inactivation rates of Ca current (see below; Kass and Tsien, 1976). In intact dog ventricular myocardium (Moore et al., 1965), the tissue exhibiting a prominent notch (close to the epicardium) had a shorter action potential than the tissue without a notch (close to the endocardium). In dog ventricular myocytes, when I_{to1} was blocked with 4-AP (Fig. 5*A*) or inactivated by a holding potential sufficiently negative not to inactivate Ca current (−50 to −40 mV; Tseng, G.-N., and B. F. Hoffman, manuscript submitted for publication), the action potential was prolonged. A similar effect of transient outward current on the action potential duration also has been noted by others (Kukushkin et al., 1983; Giles and van Ginneken, 1985; Josephson et al., 1984*b*). In sheep Purkinje

fibers, when the stimulation rate or rhythm is changed, there is a close temporal relationship between the changes in transient outward current and in the notch (Boyett, 1981). In dog ventricular myocytes, however, the time course of recovery is different for the transient outward current and the notch: the transient outward current recovered with a halftime ($t_{1/2}$) of 250 ms at a holding potential of −70 mV and the notch recovered with a $t_{1/2}$ of 1,300 ms at a resting potential of −90 mV. The discrepancy may be due to the recovery time course of I_{Ca}: in dog ventricular myocytes, at a V_h negative to −70 mV, I_{Ca} shows a biphasic time course of recovery from inactivation: it increases to a level higher than control before returning to control during recovery (Tseng and Hoffman, 1987). This would shift the early plateau to a more positive voltage and decrease the notch, even though I_{to1} has already recovered to the control level. I_{to2} seemed to contribute less to the notch than I_{to1} (Fig. 5*A*). Since I_{to2} is dependent on intracellular Ca, it is possible that an elevation in the intracellular Ca level will enhance I_{to2}, thus making the initial plateau voltage less positive, decreasing the activation of Ca current, and decreasing the Ca influx.

Ca Current

The Ca current was recorded with the whole-cell clamp method (Hamill et al., 1981), which is reported to be adequate for this purpose (Matsuda and Noma, 1984). The Ca current was isolated from the Na current and the transient outward current either by using Na-free (choline-substituted) and K-free external solution and Na-free and K-free (Cs-substituted) internal solution, or by using a holding potential of −45 mV or more positive to inactivate the Na and transient outward currents (Weidmann, 1955; Tseng et al., 1986). The delayed rectifier current could be distinguished from the Ca current because their time courses differed markedly: the inactivation time constant for the Ca current was between 10 and 60 ms (Fig. 8), while the faster activation time constant for the delayed rectifier current was between 100 and 400 ms (Figs. 10 and 12). The Ca current recorded under these two conditions behaved similarly (Figs. 6 and 7).

At 2 mM $[Ca]_o$, the threshold for Ca current activation was between −40 and −30 mV; the current reached a maximum between −10 and 0 mV and had an apparent reversal between +50 and +60 mV. At 5 mM $[Ca]_o$, there was a voltage shift of 5–10 mV in the positive direction in terms of activation threshold, maximum current voltage, and reversal voltage. At 5 mM $[Ca]_o$, the activation curve of the Ca channel is sigmoidal, extending over a voltage range from −30 to −20 mV to +10 to +20 mV with a half-maximum voltage of about −10 to 0 mV. The inactivation curve extends over a voltage range from −45 to −35 mV to 0 to +10 mV with a half-maximum voltage of about −20 mV. As a result, there is an overlap between these two curves from −20 to 0 mV (Fig. 7). Such an overlap between the activation and inactivation curves of Ca current has also been reported in neonatal ventricular cells (N. M. Cohen and Lederer, 1986) and aggregates of neonatal rat heart cells (van Ginneken and Jongsma, 1983). At both 2 and 5 mM $[Ca]_o$, the current level 200–300 ms after the start of depolarization remained inward from −35 to −30 mV to +30 to +35 mV. The Ca channel blocker nisoldipine decreased the amplitudes of both the peak Ca

current and the late inward current (Fig. 6*C*), whereas isoproterenol increased the amplitudes of both (data not shown). Part of this maintained inward current component is likely to be due to the overlap between the activation and inactivation curves. Whether there is any contribution from another type of Ca channel that shows no inactivation or only very slow inactivation (Kass and Scheuer, 1982; Nowycky et al., 1985) is not certain. Since at voltages positive to 0 mV, the Ca current inactivated more slowly with more positive voltages (Fig. 8), if the voltage level during the plateau was high, then the Ca current time course would be prolonged and the action potential duration would also be prolonged. This may explain, at least in part, the action potential prolongation seen when the transient outward current was abolished with 4-AP or a holding voltage between −50 and −40 mV and the early plateau voltage during notch was elevated from −10 to 0 mV to +20 to +30 mV.

Delayed Rectifier Current

The time-dependent K current or delayed rectifier current in cardiac tissue was first characterized by Noble and Tsien (1969), who identified two components, I_{x1} and I_{x2}, with distinctly different kinetics and voltage dependences. Subsequently, Baumgarten et al. (1977) attributed I_{x2} to currents resulting from voltage-induced changes in $[K]_o$ in restricted intercellular clefts. Many other studies on the delayed rectifier current (McDonald and Trautwein, 1978; Nakayama et al., 1984; Bennett et al., 1985; Giles and van Ginneken, 1985; Gintant et al., 1986) have provided results that differ qualitatively and quantitatively, and one study attributes it entirely to the Ca current (Jaeger and Gibbons, 1985). Gintant et al. (1986) found the activation and deactivation of the delayed rectifier current in dog Purkinje cells to be described by a double-exponential process; however, they attributed the two components to two closed states of the channel.

In dog ventricular myocytes, at holding potentials between −50 and −35 mV, there was a decaying outward tail current after depolarization to voltages positive to −30 mV. The tail current amplitude increased as the depolarization pulse was made more positive and reached a plateau at +30 to +55 mV. Normalization of the tail current amplitudes resulted in a sigmoidal activation curve extending over a voltage range from −30 to +55 mV. To characterize I_x, we eliminated interference from the Na current and the transient outward current by using a relatively positive holding potential (−50 to −30 mV). We used nisoldipine (1 μM) to eliminate the Ca current without inhibiting the delayed rectifier current (Kass, 1984). That the increase in outward current during depolarization and the outward tail current after repolarization were due to the increase in conductance of a specific type of channel is clearly shown in the envelope test of I_x (Fig. 10). Both the time course of outward current development during depolarization (activation) and outward tail current decay after repolarization (deactivation) could be fitted by the sum of two exponentials. The fast time constants for both activation and deactivation were longest in a voltage range between −15 and 0 mV and decreased at more positive and more negative voltages. The slow time constants of activation and deactivation were very long (seconds) and

probably resulted from the K accumulation and depletion in the narrow extracellular space created by surface cavaeolae.

The current *I-V* relationship of I_x shows inward rectification at about −20 mV and a reversal at −67 to −75 mV (−71.3 ± 3.5 mV, mean ± SD, n = 8). These characteristics are similar to those reported for calf Purkinje fibers (Bennett et al., 1985) and rabbit atrioventricular nodal cells (Nakayama et al., 1984). The reversal potential of the delayed rectifier current was less negative than the predicted K equilibrium potential (E_K) ($[K]_o$ = 4 mM, $[K]_i$ = 145 mM, E_K = −94 mV) and justified the term "I_x" for this current. In a voltage-clamp study on multicellular dog ventricular tissue (Beeler and Reuter, 1970), only a very small and slow time-dependent K current was observed. The discrepancy between Beeler and Reuter's results and ours is probably due to the simultaneous current changes in response to more marked K accumulation and depletion in intercellular clefts or intracellular Ca or Na concentration changes in the multicellular preparation.

The properties of I_x—activating at −30 mV or more positive voltages, having a (fast) time constant of 100–400 ms, and remaining outward at voltages positive to −70 to −75 mV—make this current useful in action potential repolarization. The presence of a maintained inward (Ca) current (Figs. 6 and 7) makes a repolarizing outward current essential for repolarization. The role of the delayed rectifier current in action potential repolarization can be clearly seen in Fig. 14. Isoproterenol elevated the action potential plateau voltage by enhancing the Ca current and shortened the action potential duration by enhancing I_x, consistent with the findings in calf Purkinje fibers (Tsien et al., 1972). When I_{Ca} was abolished by nisoldipine, isoproterenol could still shorten the action potential duration, although the plateau was not changed, which is consistent with the observation of Kass (1984).

Whether isoproterenol could change the kinetics of I_{Ca} and I_x is not certain now. For the Ca current, single channel studies show that beta-receptor stimulation can increase the mean open time and decrease the mean closed time of single Ca channels, but the average inactivation time constant of the current is either not changed or is increased by a factor of 1.4 by beta-receptor stimulation (Brum et al., 1984). Inactivation of the whole-cell Ca current by intracellular Ca should also be considered. Isoproterenol can accelerate Ca current inactivation by increasing Ca influx via Ca channels on the one hand, but decelerate Ca current inactivation by increasing Ca uptake by the sarcoplasmic reticulum on the other. The net effect will depend on the balance between effects of isoproterenol on voltage-dependent inactivation, Ca influx, and Ca uptake. The mechanism of each of these effects, and thus the dose-response relationship, is not known (e.g., phosphorylation of sarcolemma vs. sarcoplasmic reticulum proteins). Therefore, the effect of isoproterenol on the kinetics of the Ca current is hard to predict. For the delayed rectifier current, our preliminary experiments show that isoproterenol does not change the faster time constant of activation and deactivation of this current, which is consistent with the findings of Bennett et al. (1986). These authors, however, report a decrease in the slower time constant of this current. We did not perform such an analysis. However, the long time

constant of this process (400–700 ms in calf Purkinje fibers [Bennett et al., 1986] and seconds in dog ventricular cells) limits the importance of this process in action potential repolarization. Isoproterenol could also increase the background outward current by either enhancing a time-independent K conductance (Gadsby, 1983) or activating the Na-K pump (Desilets and Baumgarten, 1986). This effect was evidenced by a hyperpolarization of 2–4 mV caused by isoproterenol (Fig. 14). Such an enhanced outward current could also help shorten the action potential in the presence of isoproterenol.

In conclusion, some of our results agree with predictions that could be made from data obtained in other types of cardiac preparations: (*a*) the inward rectifier current is important in determining the resting membrane potential and repolarization; (*b*) a TTX-sensitive Na current helps maintain the plateau; and (*c*) the Ca current shows fast activation, a large amplitude, and voltage- and Ca-dependent inactivation. Some interesting findings have emerged: (*a*) the relationship between the $\dot{V}_{max}$ of phase 0 and the membrane potential is more positive and steeper than that observed in many other cardiac preparations; (*b*) in dog ventricular cells exhibiting fast repolarization during phase 1 and a notch, there is a prominent transient outward current, which consists of two components, similar to the transient outward current observed in sheep Purkinje fibers; and (*c*) the delayed rectifier current is present in dog ventricular cells and plays a role in repolarization. Since many studies on the actions and mechanisms of action for interventions on cardiac tissues have used dog ventricular muscle as a model, with inferences about the changes in membrane channels drawn from voltage-clamp studies on other cardiac preparations, the unexpected observations reported here call for more careful examination and possibly new interpretations of some of the results. Future studies using dog heart or dog ventricular muscle should also take these findings into account.

The authors would like to thank Dr. A. Noma for helpful instructions, Dr. Penelope A. Boyden for discussion and suggestions, Ms. Patricia McLaughlin for preparing the ventricular myocytes, Ms. Linda Novak for preparing the manuscript, and Dr. R. Kass for kindly providing the nisoldipine.

This work was supported by grant HL-30557 from the National Heart, Lung and Blood Institute. R. B. Robinson is an Established Fellow of the New York Heart Association.

Original version received 24 July 1986 and accepted version received 4 June 1987.

REFERENCES

Attwell, D., I. Cohen, D. Eisner, M. Ohba, and C. Ojeda. 1979. The steady-state TTX-sensitive ('window') sodium current in cardiac Purkinje fibers. *Pflügers Archiv.* 379:137–142.

Baumgarten, C. M., G. Isenberg, T. F. McDonald, and R. E. Ten Eick. 1977. Depletion and accumulation of potassium in the extracellular clefts of a cardiac Purkinje fiber during voltage clamp hyperpolarization and depolarization. Experiments in sodium-free bathing medium. *Journal of General Physiology.* 70:149–169.

Beeler, G. W., and H. Reuter. 1970. Voltage clamp experiments on ventricular myocardial fibres. *Journal of Physiology.* 297:165–190.

Bennett, P., L. McKinney, T. Begenisich, and R. S. Kass. 1986. Adrenergic modulation of the

delayed rectifier potassium channel in calf cardiac Purkinje fibers. *Biophysical Journal.* 49:839–848.

Bennett, P., L. C. McKinney, R. S. Kass, and T. Begenisich. 1985. Delayed rectification in the calf cardiac Purkinje fiber. Evidence for multiple state kinetics. *Biophysical Journal.* 48:553–567.

Boyett, M. R. 1981. Effect of rate-dependent changes in the transient outward current on the action potential in sheep Purkinje fibres. *Journal of Physiology.* 319:23–41.

Brown, A. M., and A. Yatani. 1986. Ca and Na Channels in the Heart. *In* The Heart and Cardiovascular System: Scientific Foundations. H. A. Fozzard, E. Haber, R. B. Jennings, and A. M. Katz, editors. Raven Press, New York. 1:627–636.

Brum, G., W. Osterrieder, and W. Trautwein. 1984. Beta-adrenergic increase in the calcium conductance of cardiac myocytes studied with the patch clamp. *Pflügers Archiv.* 401:111–118.

Cacei, M. S., and W. P. Cacheris. 1984. Fitting curves to data. The Simplex algorithm is the answer. *BYTE.* 9:340–362.

Callewaert, G., E. Carmeliet, and J. Vereecke. 1984. Single cardiac Purkinje cells: general electrophysiology and voltage-clamp analysis of the pacemaker current. *Journal of Physiology.* 349:643–661.

Carmeliet, E., and J. Vereecke. 1979. Electrogenesis of the action potential and automaticity. *In* Handbook of Physiology: The Cardiovascular System. Vol. 1: The Heart. R. M. Berne, editor. American Physiological Society, Bethesda, MD. 269–334.

Cohen, I., D. Attwell, and G. Strichartz. 1981. The dependence of the maximum rate of rise of the action potential upstroke on membrane properties. *Proceedings of the Royal Society of London, Series B.* 214:85–98.

Cohen, N. M., and W. J. Lederer. 1986. Steady-state kinetic parameters of the calcium current (I_{Ca}) in neonatal rat single cardiac myocytes. *Biophysical Journal.* 49:175*a*. (Abstr.)

Coraboeuf, E., and E. Carmeliet. 1982. Existence of two transient outward currents in sheep cardiac Purkinje fibers. *Pflügers Archiv.* 392:352–359.

Coraboeuf, E., E. Deroubaix, and A. Coulumbe. 1979. Effects of tetrodotoxin on action potentials of the conducting system in the dog heart. *American Journal of Physiology.* 236:561–567.

Desilets, M., and C. M. Baumgarten. 1986. Isoproterenol directly stimulates the Na^+-K^+ pump in isolated cardiac myocytes. *American Journal of Physiology.* 251:H218–H225.

Gadsby, D. C. 1983. Beta-adrenoceptor agonists increase membrane K^+ conductance in cardiac Purkinje fibres. *Nature.* 306:691–693.

Gadsby, D. C., and P. F. Cranefield. 1977. Two levels of resting potential in cardiac Purkinje fibers. *Journal of General Physiology.* 70:724–746.

Giles, W. R., and A. C. G. van Ginneken. 1985. A transient outward current in isolated cells from the crista terminalis of rabbit heart. *Journal of Physiology.* 368:243–264.

Gintant, G. A., N. B. Datyner, and I. S. Cohen. 1984. Slow inactivation of a tetrodotoxin-sensitive current in canine cardiac Purkinje fibers. *Biophysical Journal.* 45:509–512.

Gintant, G. A., N. B. Datyner, and I. S. Cohen. 1986. Gating of delayed rectification in acutely isolated canine cardiac Purkinje myocytes: evidence for a single voltage-gated conductance. *Biophysical Journal.* 48:1059–1064.

Gintant, G. A., B. F. Hoffman, and R. C. Naylor. 1983. The influence of molecular form of local anesthetic-type antiarrhythmic agents on reduction of the maximum upstroke velocity of canine cardiac Purkinje fibers. *Circulation Research.* 52:735–746.

Grant, A. O., C. F. Starmer, and H. C. Strauss. 1984. Antiarrhythmic drug action. Blockade of the inward sodium current. *Circulation Research.* 55:427–439.

Hamill, O. P., A. Marty, E. Neher, B. Sakmann, and F. J. Sigworth. 1981. Improved patch clamp techniques for high-resolution current recording from cells and cell-free membrane patches. *Pflügers Archiv.* 391:85–100.

Hewett, K., M. J. Legato, P. Danilo, Jr., and R. B. Robinson. 1983. Isolated myocytes from adult canine left ventricle: Ca^{2+} tolerance, electrophysiology, and ultrastructure. *American Journal of Physiology.* 245:H830–H839.

Hilgemann, D. W. 1986. Extracellular calcium transients and action potential configuration changes related to post-stimulatory potentiation in rabbit atrium. *Journal of General Physiology.* 87:675–706.

Hoffman, B. F., and P. F. Cranefield. 1960. The ventricle. *In* Electrophysiology of the Heart. Futura Publishing Co., New York. 75–103.

Houser, S. R., A. Bahinski, and L. H. Silver. 1985. Passive membrane properties of isolated feline ventricular myocytes. *American Journal of Physiology.* 248:H622–H630.

Hume, J. R., and W. Giles. 1981. Active and passive electrical properties of single bullfrog atrial cells. *Journal of General Physiology.* 78:19–42.

Hume, J. R., and A. Uehara. 1985. Ionic basis of the different action potential configurations of single guinea-pig atrial and ventricular myocytes. *Journal of Physiology.* 368:525–544.

Iijima, T., H. Irisawa, and M. Kameyama. 1985. Membrane currents and their modification by acetylcholine in isolated single atrial cells of the guinea-pig. *Journal of Physiology.* 359:485–501.

Ikeda, K., and M. Hiraoka. 1982. Effects of hypoxia on passive electrical properties of canine ventricular muscle. *Pflügers Archiv.* 393:45–50.

Isenberg, G., and U. Klockner. 1982*a*. Isolated bovine ventricular myocytes. Characterization of the action potential. *Pflügers Archiv.* 395:19–29.

Isenberg, G., and U. Klockner. 1982*b*. Calcium currents of isolated bovine ventricular myocytes are fast and of large amplitude. *Pflügers Archiv.* 395:30–41.

Jaeger, J. M., and W. R. Gibbons. 1985. A reexamination of late outward plateau currents of cardiac Purkinje fibers. *American Journal of Physiology.* 249:H108–H121.

Josephson, I. R., J. Sanchez-Chapula, and A. M. Brown. 1984*a*. A comparison of calcium currents in rat and guinea-pig single ventricular cells. *Circulation Research.* 54:144–156.

Josephson, I. R., J. Sanchez-Chapula, and A. M. Brown. 1984*b*. Early outward current in rat single ventricular cells. *Circulation Research.* 54:157–162.

Kass, R. S. 1984. Delayed rectification in the cardiac Purkinje fiber is not activated by intracellular calcium. *Biophysical Journal.* 45:837–839.

Kass, R. S., and T. Scheuer. 1982. Slow inactivation of calcium channels in the cardiac Purkinje fiber. *Journal of Molecular and Cellular Cardiology.* 14:615–618.

Kass, R. S., and R. W. Tsien. 1976. Control of action potential duration by calcium ions in cardiac Purkinje fibers. *Journal of General Physiology.* 67:599–617.

Kenyon, J. L., and W. R. Gibbons. 1979. 4-Aminopyridine and the early outward current of sheep cardiac Purkinje fibers. *Journal of General Physiology.* 73:139–157.

Kukushkin, M. I., R. Z. Gainullin, and E. A. Sosunov. 1983. Transient outward current and rate dependence of action potential duration in rabbit cardiac ventricular muscle. *Pflügers Archiv.* 399:87–92.

Litovsky, S., and C. Antzelevitch. 1986. The transient outward current. Canine epicardium vs. endocardium. *Circulation.* 74(Suppl.):II–255.

Matsuda, H., and A. Noma. 1984. Isolation of calcium current and its sensitivity to monovalent cations in dialyzed ventricular cells of guinea-pig. *Journal of Physiology.* 357:553–573.

McDonald, T. F., and W. Trautwein. 1978. The potassium current underlying delayed rectification in cat ventricular muscle. *Journal of Physiology.* 274:217–246.

Moore, E. N., J. B. Preston, and G. K. Moe. 1965. Durations of transmembrane action potentials and functional refractory periods of canine false tendon and ventricular myocardium: comparisons in single fibers. *Circulation Research.* 17:259–273.

Nakayama, T., and H. Irisawa. 1985. Transient outward current carried by potassium and sodium in quiescent atrioventricular node cells of rabbits. *Circulation Research.* 57:65–73.

Nakayama, T., Y. Kurachi, A. Noma, and H. Irisawa. 1984. Action potential and membrane currents of single pacemaker cells of the rabbit heart. *Pflügers Archiv.* 402:248–257.

Noble, D. 1980. The Initiation of the Heartbeat. Clarendon Press, Oxford. 167 pp.

Noble, D., and R. W. Tsien. 1969. Outward membrane currents activated in the plateau range of potentials in cardiac Purkinje fibres. *Journal of Physiology.* 200:205–231.

Nowycky, M. C., A. P. Fox, and R. W. Tsien. 1985. Three types of calcium channels in chick dorsal root ganglion cells. *Biophysical Journal.* 49:67*a*. (Abstr.)

Powell, T., and V. W. Twist. 1976. A rapid technique for the isolation and purification of adult cardiac cells having respiratory control and tolerance to calcium. *Biochemical and Biophysical Research Communications.* 72:327–333.

Reimer, K. A., and R. B. Jennings. 1986. Myocardial Ischemia, Hypoxia, and Infarction. *In* The Heart and Cardiovascular System: Scientific Foundations. H. A. Fozzard, E. Haber, R. B. Jennings, and A. M. Katz, editors. Raven Press, New York. 2:1133–1202.

Sakamoto, Y., and M. Goto. 1970. A study of the membrane constants in the dog myocardium. *Japanese Journal of Physiology.* 20:30–41.

Sakmann, B., and G. Trube. 1984. Conductance properties of single inwardly rectifying potassium channels in ventricular cells from guinea-pig heart. *Journal of Physiology.* 347:641–657.

Sheets, M. F., C. T. January, and H. A. Fozzard. 1983. Isolation and characterization of single canine cardiac Purkinje cells. *Circulation Research.* 53:544–548.

Siegelbaum, S. A., and R. W. Tsien. 1980. Calcium-activated transient outward current in calf cardiac Purkinje fibres. *Journal of Physiology.* 299:485–506.

Solberg, L. E., D. H. Singer, R. E. Ten Eick, and E. G. Duffin. 1974. Glass microelectrode studies on intramural papillary muscle cells. Description of preparation and studies on normal dog papillary muscle. *Circulation Research.* 34:783–797.

Sutko, J. L., and J. L. Kenyon. 1983. Ryanodine modification of cardiac muscle responses to potassium-free solutions. Evidence for inhibition of sarcoplasmic reticulum calcium release. *Journal of General Physiology.* 82:385–404.

Trautwein, W. 1973. Membrane currents in cardiac muscle fibers. *Physiological Reviews.* 53:793–835.

Tseng, G.-N., and B. F. Hoffman. 1987. A novel mechanism controlling Ca current repriming in mammalian ventricular cells. *Biophysical Journal.* 51:410*a*. (Abstr.)

Tseng, G.-N., R. B. Robinson, and B. F. Hoffman. 1986. Two components of transient outward current in canine ventricular myocytes. *Biophysical Journal.* 49:53*a*. (Abstr.)

Tsien, R. W., W. Giles, and P. Greengard. 1972. Cyclic AMP mediates the effects of adrenaline on cardiac Purkinje fibres. *Nature New Biology.* 240:181–185.

van Ginneken, A. C. G., and H. J. Jongsma. 1983. Slow inward current in aggregates of

neonatal rat heart cells and its contribution to the steady state current-voltage relationship. *Pflügers Archiv.* 397:265–271.

Watanabe, T., P. M. Rautaharju, and T. F. McDonald. 1985. Ventricular action potentials, ventricular extracellular potentials, and the ECG of guinea pig. *Circulation Research.* 157:362–373.

Weidmann, S. 1955. The effect of the cardiac membrane potential on the rapid availability of the sodium-carrying system. *Journal of Physiology.* 127:213–224.